CORA Cork Open Research Archive
Cartlann Taighde Oscailte Chorcaí

Title	Enhanced catalytic activity of high index faceted palladium nanoparticles in Suzuki-Miyaura coupling due to efficient leaching mechanism
Authors	Collins, Gillian;Schmidt, Michael;O'Dwyer, Colm;McGlacken, Gerard P.;Holmes, Justin D.
Publication date	2014-07-30
Original Citation	COLLINS, G., SCHMIDT, M., O'DWYER, C., MCGLACKEN, G. & HOLMES, J. D. 2014. Enhanced Catalytic Activity of High-Index Faceted Palladium Nanoparticles in Suzuki–Miyaura Coupling Due to Efficient Leaching Mechanism. ACS Catalysis, 4, 3105-3111. http://pubs.acs.org/doi/abs/10.1021/cs5008014
Type of publication	Article (peer-reviewed)
Link to publisher's version	http://pubs.acs.org/journal/accacs - 10.1021/cs5008014
Rights	© 2014 American Chemical Society. This document is the Submitted Manuscript version of a Published Work that appeared in final form in ACS Catalysis, copyright © American Chemical Society after peer review and technical editing by the publisher. To access the final edited and published work see http://dx.doi.org/10.1021/cs5008014
Download date	2024-03-29 00:33:52
Item downloaded from	https://hdl.handle.net/10468/2279

UCC
University College Cork, Ireland
Coláiste na hOllscoile Corcaigh

Enhanced Catalytic Activity of High Index Faceted Palladium Nanoparticles in Suzuki-Miyaura Coupling due to Efficient Leaching Mechanism

*Gillian Collins[†, ϕ], Michael Schmidt, Colm O'Dwyer[†,§,] Gerard McGlacken[†, *], and Justin Holmes[†, ϕ, *]*

[†]*Department of Chemistry Department and the Tyndall National Institute, University College Cork, Cork, Ireland.*

[ϕ]*Centre for Research on Adaptive Nanostructures and Nanodevices, Trinity College, Dublin, Ireland*

[§]*Materials and Surface Science Institute, University of Limerick, Limerick, Ireland.*

*To whom correspondence should be addressed: Tel: +353 (0)21 4903608; Fax: +353 (0)21 4274097; E-mail: j.holmes@ucc.ie

Abstract

The structure-property relationship of palladium (Pd) catalysts in Suzuki-Miyaura cross coupling reactions was investigated using Pd nanocrystals of uniform size and shape. Superior catalytic reactivity was observed for Pd nanoparticles with high index {730} surface facets compared to low index {100} facets. While the nanocrystal morphologies were maintained during the reaction, the presence of leached Pd clusters, identified by high resolution transmission electron microscopy (TEM), indicate a homogenous process. The nature of the surface facets on the nanoparticles were observed to influence the rate of Pd leaching during the Suzuki coupling reaction. The enhanced reactivity observed for the high index facet catalysts stems from the greater number of leachable atoms of low abstraction energy available on high index planes.

Introduction

Noble metal nanocrystals with high index surface facets have attracted much interest due to their potential for enhanced catalytic performance.[1] High index facets are denoted by a set of Miller indices {*hkl*}, where one index is greater than one. Unlike low index planes characterized by such as {111} and {100} facets, which are relatively smooth, the surface atomic structure of high index facets are characterized by a high density of step, terrace and kink sites.[2] Such surfaces are well known to improve catalytic rates for many reactions.[3] The physical origins of structure sensitivity are complex and generally ascribed to electronic and geometrical effects that influence adsorption energies and reaction pathways.[4] Chemisorption of reaction species can be preferential on step and kink sites due to their low co-ordination numbers (6-7) or allow more energetically favorable transition states compared to close-packed surfaces[5].

Pd is an important noble metal as a heterogeneous catalyst for chemical synthesis, automotive and fuel cell applications.[6-7] Pd is the principle catalyst metal for carbon-carbon cross coupling reactions which are central to a variety of chemical processes for pharmaceutical and fine chemicals industries.[8] The versatile nature of these reactions has also lead to many other applications such as the surface modification of semiconductors[9], the preparation of inorganic-organic nanocomposites[10] and sensors.[11] Coupling reactions conventionally use homogenous catalysts but heterogeneous nanoparticle-based catalysts are attractive as they offer convenient removal of the catalyst post reaction. The possibility of recovery and recyclability of the catalyst also makes them more economically attractive, especially for expensive noble metals. A variety of coupling reactions including Suzuki-Miyaura, Heck, Ullman, Stille and Sonogashira, all proceed under heterogeneous conditions.[6, 12-14] Suzuki coupling reactions are one of the most widely utilized methods for the construction of carbon-carbon bonds and are very effective under heterogeneous conditions.[12] Suzuki coupling of

aryl chlorides, even deactivated ones, can be achieved under heterogeneous conditions, which are desirable for industrial synthesis due to the low cost of chloride starting materials.[14-16]

A wide variety of heterogeneous catalysts have been studied for Suzuki coupling including dispersed nanoparticles,[17-18] powder-supported nanoparticles[19-21] and catalytic thin films.[22 23] Several studies have demonstrated considerably enhanced catalytic performance of Suzuki reactions when using nanocrystals enclosed by high index surface facets.[24-28] A variety of preparation methods have been reported for Pd nanocrystals with high index surface facets such as seeded growth[26], epitaxial growth[25, 29] and electrochemically[30-32] and solid state methods.[33] The origin of the enhanced reactivity observed is generally attributed the high density of low-coordinate atoms present at the surface of the catalyst.[2] Early reports of heterogeneously catalyzed Suzuki coupling suggest a surface driven reaction occurring at the edge and corner sites of nanoparticles[34-35] and this hypothesis is supported by a number of studies providing evidence of a surface mediated process.[36-38] If a reaction occurs preferentially at edge sites then enhanced reactivity reported for high index planes compared to low index planes would be reasonable due to the stepped nature of the high index facets. A considerable number of mechanistic studies have identified that leaching processes occur in many nanoparticle catalyzed reactions.[39-41] Although debate still surrounds the leaching mechanism, dissolved Pd from the nanoparticle surface has been shown to play a central role in the catalytic cycle of Suzuki reactions. [42-43]

Herein, we investigate the structure-property relationship of catalysts in Suzuki cross coupling reactions using Pd catalysts of uniform size and shapes. The catalytic reactivity of Pd nanoparticles with low index {100} facets and high index {730} facets are compared. A considerably improved catalytic performance was observed from high index nanocrystals. Catalytic studies, high resolution electron microscopy and XPS analysis was used to elucidate the mechanism of the enhanced reactivity associated with the high index surface planes. We

identify that the superior activity observed for the high index faceted catalysts stems from the greater leaching of Pd atoms from the surface rather than a true surface-mediated process.

Experimental

Pd Nanocrystal Synthesis: Cubic nanocrystals with edge lengths of 10 and 20 nm were synthesized as previously described and used for the seeded growth of the concave nanocrystals.[26] These nanoparticles are capped with PVP and Br capping ligands. To avoid the influence of support materials on the catalytic activity of the nanocrystals, unsupported nanoparticles were used.

Materials Characterization: Scanning electron microscopy (SEM) images were obtained using a FEI DualBeam Helios NanoLab 600i high resolution SEM. Transmission electron microscopy (TEM) analysis was performed using a Jeol 2100 electron microscope at an operating voltage of 200 kV. X-ray Photoelectron Spectroscopy (XPS) was acquired using a KRATOS AXIS 165 monochromatized X-ray photoelectron spectrometer equipped with an Al Kα (hv = 1486.6 eV) X-ray source. Spectra were collected at a take-off angle of 90° and all spectra were reference to the C 1s peak at 284.6 eV.

Catalytic studies: In a typical reaction, 0.268 g of phenylboronic acid (2.2 mmol). 0.468 g of 4-methoxyiodobenzene or 0.25 ml of 4- methoxybromobenezene (2 mmol), 0.553 g (4 mmol) of K_2CO_3 were added to 30 ml of ethanol/water (3:1). The reactions were initiated by addition of the catalyst. Reactions were conducted at room temperature and sampled at regular intervals for GC analysis. Samples were analyzed using an Agilent 7890A GC system, equipped with a flame ionization detector (FID). Products were identified against authenticated standards and quantified by calibration to obtain response factors (RF) against the known internal standard (dodecane). The turnover number (TON) and turn over

frequency (TOF) were calculated based on the amount of biaryl product formed. The TON^{surf} and TOF^{surf} are the TON and TOF normalized to the number of surface Pd atoms. The number of surface atoms on cubic and concave cubic nanocrystals was calculated based geometrical considerations assuming a face centred cubic (fcc) Pd lattice. The total number of Pd atoms per nanocrystal was estimated by the volume of a cube or concave cube/volume of the unit cell ($3\sqrt{a}$) × number of atoms per unit cell (4), where a is the lattice constant for fcc Pd, taken to be 0.389 nm. The total number of surface atoms was estimated by: surface area of the cube/surface area of the 2 dimensional lattice × 2. For concave cubes, this relationship was multiplied by 3/7 assuming the atomic density of the {730} surface facets is three-sevenths that of the {100} facets. The volume of a concave cube was approximated by taking the volume of a cube minus the volume of the square pyramids occupying the 6 sides of a cube.

Results and Discussion

Figures 1 (a) and (c) show TEM images of cubic nanocrystals enclosed by 6 {100} surface facets, with closed packed atoms and a surface atom co-ordination number of 8. Figure 1(b) shows a TEM image of concave cubic Pd nanocrystals that measure 20 nm across and 35 nm from corner to corner. Based on the projection of angle along the [44] direction, the faces can be indexed to the {730} surface facet, as shown in figure 1 (d). [44] A {730} facet consists of a periodic series of two (210) facets and one (310) facet, as illustrated in the TEM in figure 1(e) and the schematic in figure 1(f). The density of step surface atoms is ~5×10^{-14} cm^{-2}, which implies that about 40 % of surface atoms are located at step sites. The catalytic performance of the low and high index surface planes was compared in the cross coupling of

4-methoxyiodobenzene (1) acid and phenylboronic (2) in EtOH/H_2O, as illustrated in scheme 1.

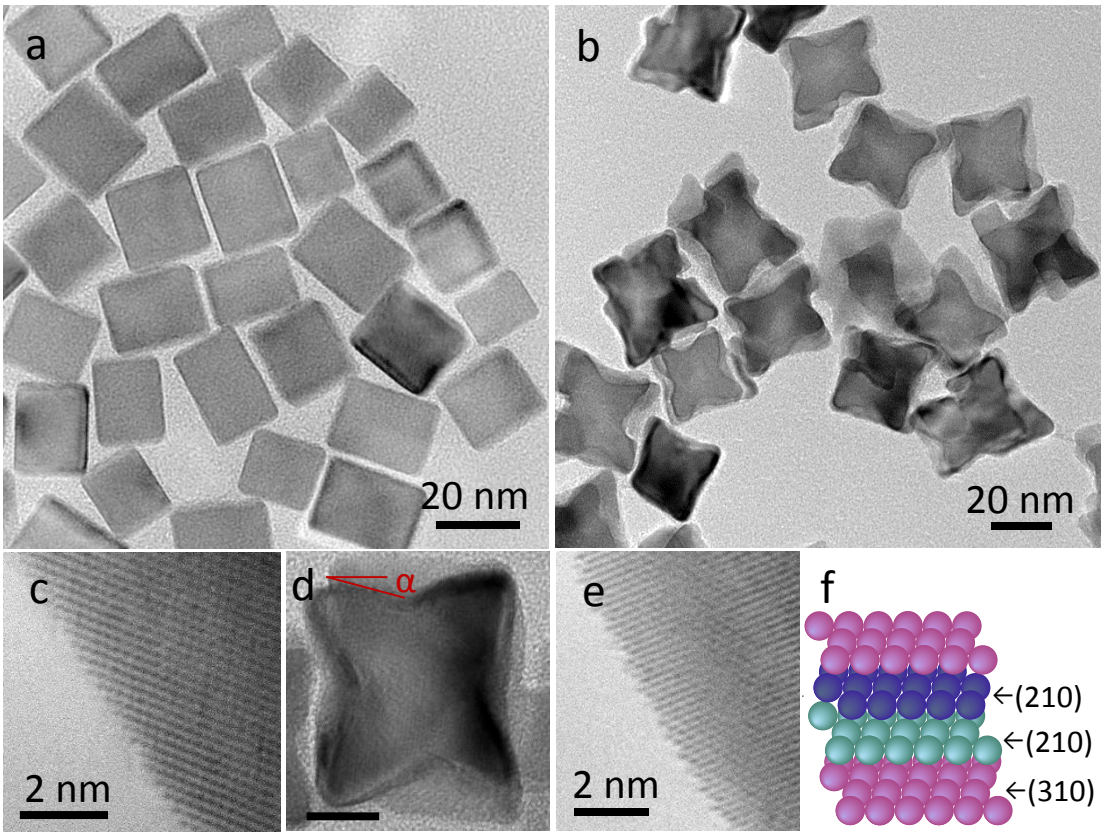

Figure 1. TEM image of as-synthesized (a) 20 nm cubic Pd NCs, (b) concave cubic Pd nanocrystals. (c) Surface of cubic nanocrystals, (d) concave cubes, (e) surface of concave cubic nanocrystals and (f) schematic illustrating the {730} facet. Scale bar figure (d) is 10 nm.

Scheme 1. Model Suzuki-Miyaura reaction used in this study.

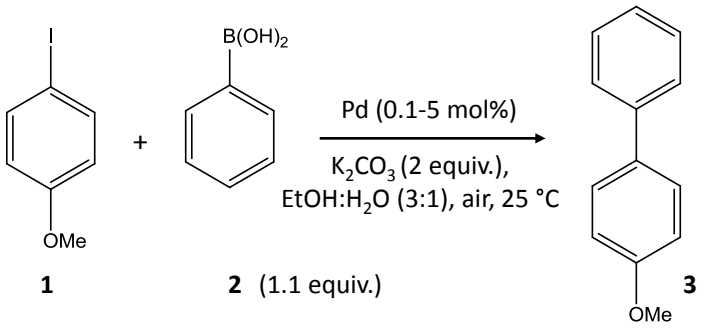

Figure 2 shows the reaction profiles for cubic (10 nm and 20 nm) and concave cubic nanocrystals and reveals significant differences in the catalytic behavior with both size and shape effects observed in the catalytic activity. The concave cubes and 10 nm cubic catalysts were found to be active for the coupling reaction while the 20 nm cubic nanocrystals showed no reactivity, at a Pd concentration of 0.5 mol%. The enhanced catalytic activity of the high index surface facets is apparent, with the yield of biphenyl product increasing from 54 % for cubic catalysts to 92 % for concave cubic catalyst. This reactivity represents a 7-fold increase in the TON for the high index surfaces (TON = 7077) compared to low index planes (TON = 1073), after normalization to the number of surface atoms for each nanocrystal. Both the 10 nm and 20 nm cubic catalysts were found to be inactive for the coupling of 4-methoxybromobenzene and phenylboronic acid, while concave cubes displayed similar reactivity as the aryl iodides achieving an 89 % yield. No induction period was observed for the concave cubes, whereas the reaction catalyzed by the cubic catalysts displayed a considerable lag time of 300 min.

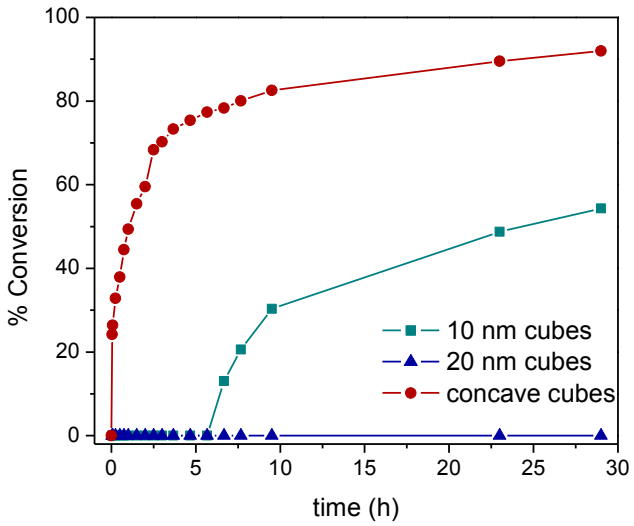

Figure 2. Reaction profile of Suzuki coupling reactions using Pd nanocrystals with high and low index facets.

Figures 3 (a) and (b) show SEM images of the cubic and concave cubic catalysts collected after the reaction, respectively. The catalysts showed negligible change to their morphology and the well-defined surface facets were interact, as shown by the inset TEM images. While the nanocrystals showed little change to their shape, detailed TEM analysis revealed the presence of small nanoparticles about 1-2 nm in diameter, in the Pd residue collected after the reaction, as shown in figures 3 (c) and (d). High resolution imaging of these particles, shown in figures 3 (c) and (d) insets, indicates a d spacing of 0.23 nm, which can be attributed to Pd(111) lattice fringes.[22] Pd clusters are observed in the TEM grids of both low index and high index particles. These particles were not present in the as-synthesized solution of the catalyst nanocrystals and so can attributed to leached Pd during the reaction.[45] Notabaly, Pd clusters of 1-2 nm in diameter only comprise ~200-300 atoms, which accounts for about 0.4 % of the total atoms in a 10 nm cubic nanocrystal. Significant changes to the nanocrystal morphology was not readily apparent at high catalyst concentrations (0.5 mol%), consistent with previous reports.[26] When the Pd catalyst concentration is decreased to 0.1 mol%, after

24 hour reaction at room temperature, dissolution of the concave cubic structures are clearly observed as shown in figure 3 (d).

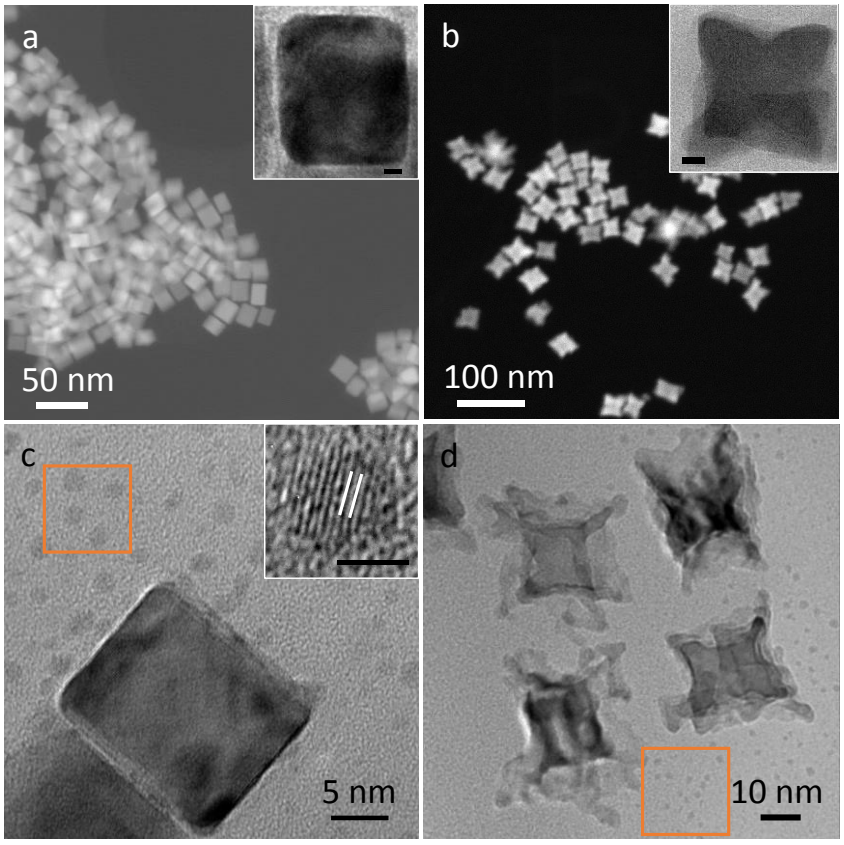

Figure 3. SEM image of cubic Pd NCs and (b) concave cubic Pd NCs cubes after a Suzuki coupling reaction (0.5 mol%) The insets in (a) and (b) show TEM images of the individual nanocrystals. Scale bars in insets are 2 nm. (c) TEM image of cubic NCs and (d) concave NCs Pd 0.1 mol% after the reaction showing the presence of small diameter Pd nanoparticles. The scale bar insets of (c) and (d) are 2 nm.

The effect of catalyst concentration was assessed and figure 4 shows the reaction profiles of cubic and concave cubic nanocrystals with a Pd concentration of 0.1, 0.5, 1 and 5 mol%. The TONs and TOFs for the different catalyst concentrations are shown in table 1. Cubic nanocrystals (figure 4 (a)) displayed an increased conversion rate with increasing Pd concentration. No conversion was observed with a Pd concentration of 0.1 mol%. Similarly, while the 20 nm cubic nanocrystals (figure 4 (b)) gave no conversion at 0.5 mol%, yields of 32% and 48% could be achieved with 1 and 5 mol% Pd, respectively. Interestingly, the concave cubic catalysts did not exhibit the same reactivity trend, with varying catalyst concentration. As shown in figure 4(c), a Pd concentration of 1 mol% was faster than a higher catalyst concentration of 5 mol%. Figure 4(d) shows a magnification of the first 180 min of the reaction, illustrating that initially the 5 mol% displayed the fastest conversion, but the reaction slowed as it progressed. This inverse relationship between the Pd concentration and rate has been associated with a homogenous mechanism.[44] Deactivation of this so-called *homeopathic* Pd occurs as the solubilized Pd nucleates to form Pd clusters that continue to grow.[46-47] Quenching of the catalytically active Pd atoms in solution becomes more efficient as the Pd concentration increases due to greater leaching. TEM analysis also provided evidence for this deactivation mechanism at higher Pd concentrations, which showed the presence of Pd aggregates compared to discreet nanoparticles observed at lower Pd concentrations (Supporting Information Figure S1).

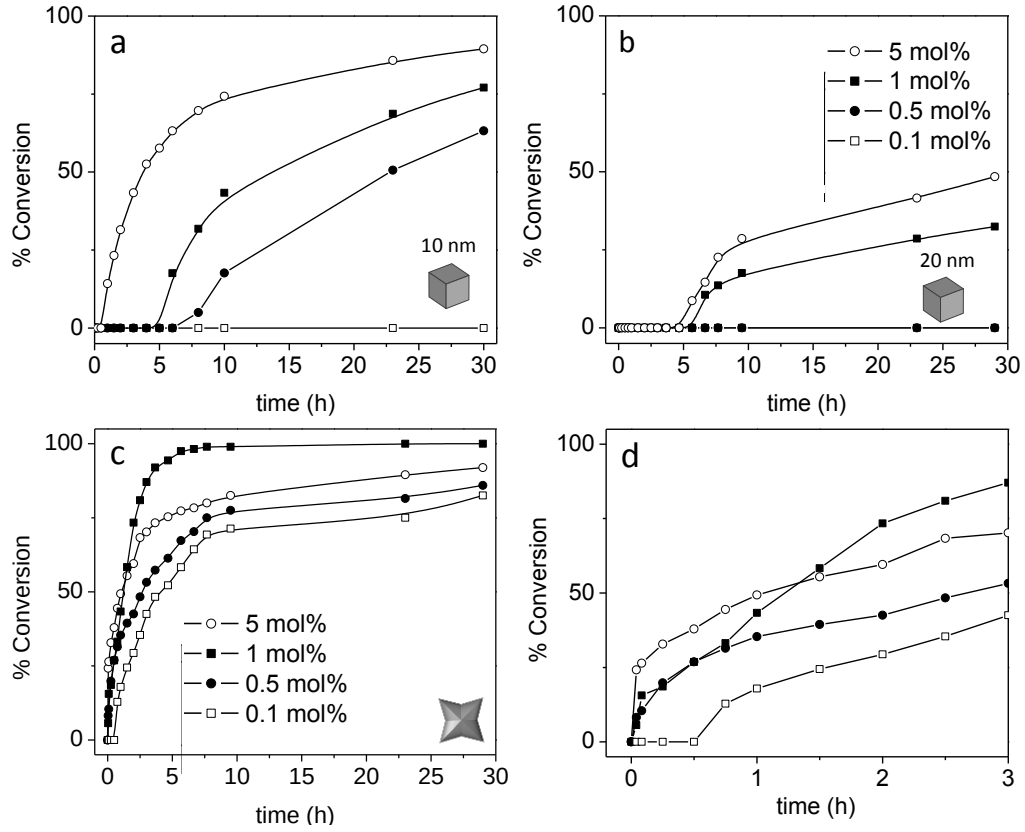

Figure 4. Reaction profile with varying Pd concentrations for (a) 10 nm cubic nanocrystals, (b) 20 nm cubic nanocrystals and (c) and (d) concave cubic nanocrystals.

Table 1. Effect of catalyst concentration for cubic and concave cubic nanocrystals in Suzuki coupling.

Catalyst	**Yield**	**Time**	**TON^{tot}**	**TON^{surf}**	**TOF^{surf}**
mol%	**%**	**h**			
Cube (10 nm)					
0.1	0	30	0	0	0
0.5	59	30	118	1073	38
1	77	30	77	700	23
5	89	30	17.8	161	5

Cube (20 nm)					
0.1	0	30	0	0	0
0.5	0	30	0	0	0
1	32	30	32	533	18
5	48	30	9.6	160	5.3
Concave cube					
0.1	72	9.5	720	28000	3032
0.5	89	9.5	178	6846	721
1	100	9.5	100	4000	133
5	83	9.5	16.6	638	67

*See Experimental section for calculation of TOFs.

A significant difference in the catalytic behavior is the absence of an induction period for the high index nanocrystals and a very long induction time for the cubic nanocrystals. Lag periods have been attributed to the time required to leach sufficient Pd into solution for catalytic turnover. Based on the TEM analysis indicating a homogeneous mechanism, the absence of an induction period for the concave cubic nanocrystals suggests rapid leaching from the nanocrystal surfaces. To investigate if the induction time was associated with Pd leaching the reaction catalyzed by the cubic nanocrystals was stopped after 60 min, by which time no biphenyl product was formed, the presence of Pd clusters was not observed by TEM analysis. In comparison, when the reaction catalyzed by the concave cubic nanocrystals was stopped after 60 min, when conversion is at 38%, the presence of the leached Pd clusters were observed by TEM (Supporting Information Figure S2). While TEM cannot quantify the leached Pd, it qualitatively shows that the presence of leached Pd, in the form of molecular or clusters, play a central role in the catalytic activity.

To further investigate the reaction regents that contribute to leaching, the cubic nanocrystals (0.5 mol %), which have a long induction period, were pre-stirred separately in solutions of the aryl iodide, boronic acid + K_2CO_3, K_2CO_3 and EtOH:H_2O for 3 hours, after which time the remaining reagents were added. The reaction profiles were monitored to determine if the conversion rates improved due to leaching. Figure 5 compares the reaction profiles of the pre-stirred solutions and a control reaction where no pre-stir was conducted. All of the pre-stirred solutions except the EtOH:H_2O solvent exhibited faster reactions, with the base and boronic acid having the most influence, increasing the yield to 90% from 59% without the pre-stir. The faster conversion was observed for the pre-stir samples suggesting leaching of Pd occurs and that all the agents can promote leaching to some degree. Much debate surrounds the leaching mechanism, with oxidative addition of the aryl halide being common for organic solvents[40], while the base and boronic acid promote leaching under aqueous conditions.[42]

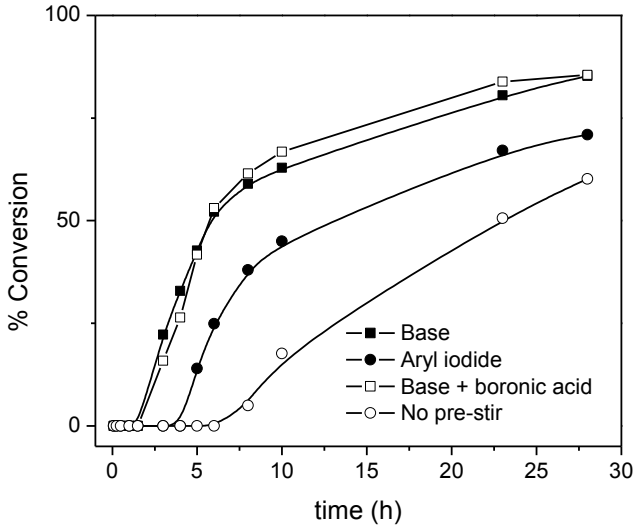

Figure 5. The influence of pre-stirring cubic catalysts in solutions of K_2CO_3, 4-methoxyiodobenzene, K_2CO_3 + phenylboronic acid. Nanocrystals pre-stirred in EtOH:H_2O showed no difference to the control and is omitted for clarify.

The effect of the individual reagents on the morphology of the cubic catalysts, stirred separately in EtOH:H_2O solutions of 4-methoxyiodobenzene, phenylboronic acid + K_2CO_3, K_2CO_3 and phenylboronic acid, was also assessed by TEM. After 24 h, the nanoparticles were collected and analyzed by TEM as shown in figure 6. Stirring the aryl halide left the cubic morphology excellently preserved (figure 6 (a)) and the presence of Pd clusters was not readily apparent. A mixture of boronic and base also left the cubic shape intact but the presence of small diameter (1-2 nm) Pd nanoparticles were readily identified, similar to that observed in the post reaction mixture. Finally, stirring the catalysts in the presence of the base alone caused no significant change in morphology and no Pd clusters were observed by TEM (Supporting Information figure S4). Interestingly, the boronic acid alone has the most significant influence on the morphology of the nanocrystals; the concave cubic nanocrystals lost their defined edges becoming more spherical as shown in figure 6(c). Many of the cubic nanocrystals dissolved and the catalysts became spherical. The diameter of these particles was larger (5-10 nm) than those observed when the nanocrystals are stirred in boronic acid + K_2CO_3. Unlike the base or aryl halide, the boronic acid can act as both a reducing agent for the leached Pd and a capping ligand that facilitates the formation of Pd nanoparticles.[48]

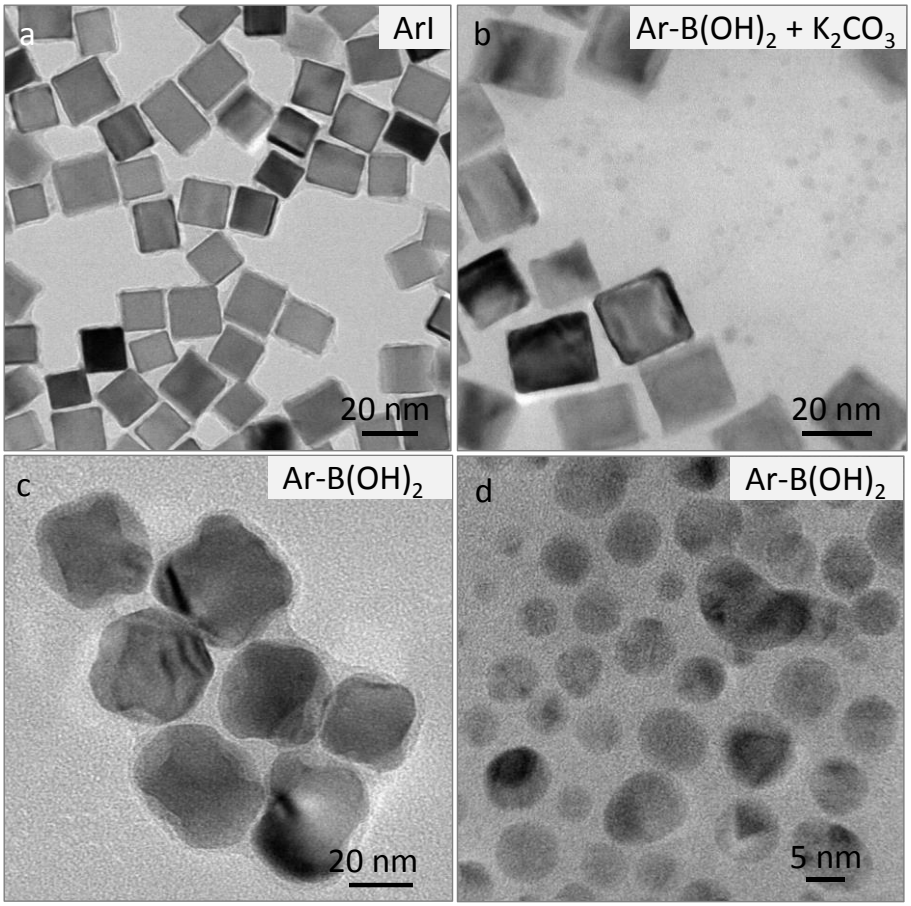

Figure 6. TEM images of cubic NCs after stirring in (a) MeO-Ph-I, (b) phenylboronic acid and K_2CO_3 (c) concave NCs and (d) cubic NCs stirred in phenylboronic acid.

Filtration tests are commonly used to assess the homogeneity of heterogeneity of the reaction mechanism, although it has been noted that redisposition of the leached Pd make them unreliable.[49] Figure 7 (a) shows the reaction profile catalyzed by concave cubes when the reaction mixture was filtered through activated carbon and washed with EtOH:H_2O, 90 min after the reaction was initiated. Comparison with the non-filtrated reaction clearly show that formation of the biaryl product stops after filtration. This loss of catalytic activity can be attributed to the removal of both the parent nanocrystal and the Pd clusters formed due to leaching. TEM analysis of the activated carbon confirmed the capture of Pd clusters in addition to the concave cubes by filtration as shown in figure 7 (b) and (c). TEM analysis of

the centrifuged filtrates did not contain Pd clusters which were present in the non-filtered samples. It is worth noting that although leaching is identified as an important step in the catalytic activity of the nanocrystals, it does not identify the nature of the catalytic species *i.e.* if the reaction is catalyzed by molecular Pd or the small diameter clusters observed by TEM.

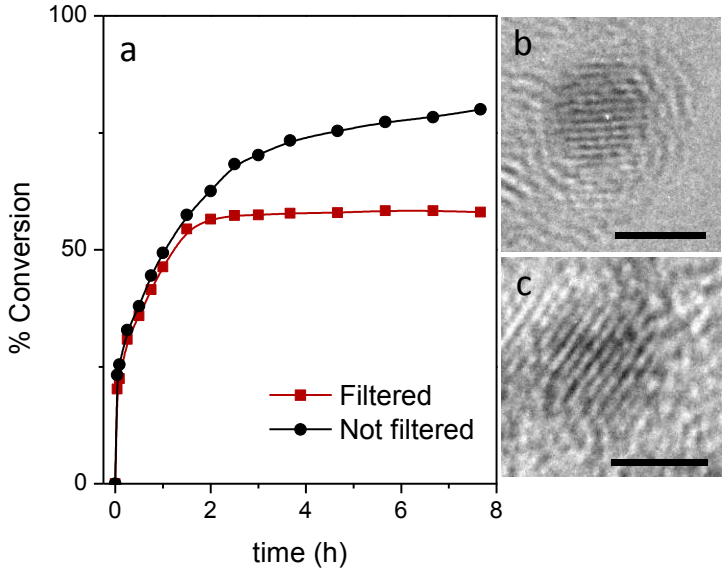

Figure 7. (a) Reaction profile of Suzuki coupling reactions catalyzed by concave Pd nanocrystals showing the effect of filtration 90 min into the reaction. (b)-(c) TEM image of Pd clusters captured on activated carbon after reaction filtration. Scale bar = 2nm.

XPS analysis was used to determine if leaching gave rise to changes in the nanocrystal surface chemistry. Figure 8 shows the Pd 3d core level of the cubic nanocrystals before and after the reaction. Before the reaction, the nanocrystals primarily consisted of metallic Pd, as indicated by the Pd(0) peak at a binding energy of 335.1 eV. The small shoulder peak located at a binding energy of 336.1 eV is typically assigned to surface and bulk PdO.[50] Figure 9(b) shows the Pd spectrum after the reaction, with an increased intensity of the PdO_2 peak. The formation of surface oxide is consistent with the presence of Pd clusters, which

undergo surface oxidation in the absence of stabilizing ligands. The survey spectra shows the presence of the N 1s peak at 400 eV, indicating that the PVP capping layer is maintained and no variation in the Pd:N ratio was observed before and after the reaction (Supporting Information Figure S4).

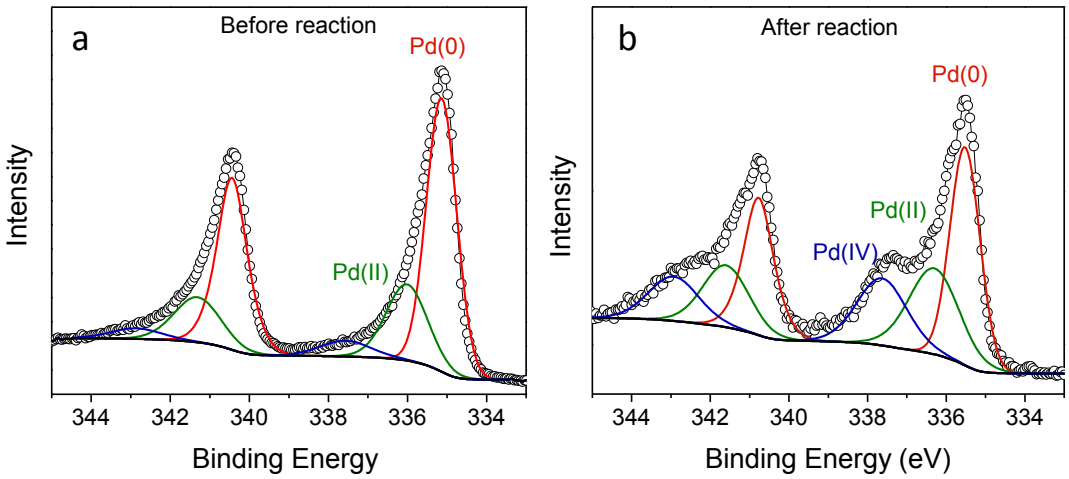

Figure 8. Pd 3d core level spectra of cubic NCs (a) before the reaction and (b) after the reaction. Spectrum (b) was collected using Pd catalysts from several reactions.

The data obtained from the present study correlate well with the catalytic leaching mechanism, although the contribution of a heterogeneous mechanism cannot be completely ruled out. The significant difference in catalytic activity between the high and low index facet nanocrystals suggests that leaching is the rate determining step in this study. Atom abstraction energies for a 3 nm spherical Pd nanoparticles were calculated to be 45 kcal mol^{-1}.[51] Atoms with lower co-ordination numbers, such as vertex and edge atoms, have lower abstraction energies compared to face atoms. Computational modelling of nanoparticle catalyzed Suzuki coupling reactions are lacking, however density functional theory (DFT) calculations based on homogenous catalysts determine the typical activation energies for

oxidative addition of aryl iodides and transmetalation to be 20-25 kcal mol^{-1}.[52-53] The relatively high activation energies for Pd leaching support the consensus that leaching is the rate-determining step. The surface atomic structure influences the stability and leaching susceptibility of Pd atoms and consequently catalytic activity. There are formally no step sites on {100} surfaces, while 42% of the atoms on a {730} surface are step sites, therefore the concave cubes have a high number of leachable atoms with lower abstraction energy compared to the cubic nanocrystals. In the Suzuki reaction the higher surface step atom density of the concave cubic catalysts facilitates more efficient leaching leading to the superior catalytic performance. The rapid leaching resulted in no measureable induction period for reactions involving concave cubic Pd nanocrystal catalysts. In contrast, a long lag time was observed with cubic nanocrystals reflecting the slower leaching from closed packed surfaces.

Conclusions

Pd nanocrystals with high index surface facets display superior catalytic performance in Suzuki coupling reactions compared to low index faces. The origin of enhanced catalytic activity associated with catalysts enclosed by high index surfaces was investigated. TEM analysis identified the presence of small diameter Pd clusters in solution after the reaction, indicating a homogenous leaching mechanism. These Pd clusters were only observed after the formation of biphenyl *i.e.* not observed during the induction period. The high number of surface atoms located at step sites on the concave cubic nanocrystals make it more energetically favorable to leach atoms from high index surface facets compared to closed packed surfaces on cubic nanocrystals. These results provide a greater understanding into the structure-property relationships of noble metal catalysts and can further facilitate design of heterogeneous catalysts for specific reactions.

Acknowledgments

We thank Enterprise Ireland (grant EI2011-0139) and Eli Lilly for supporting this research. We also acknowledge financial support from Science Foundation Ireland under award 08/CE/I1432.

Supporting Information Available

TEM images of leached Pd nanoparticles in the reaction solution and the XPS survey spectra of concave and cubic catalysts after reaction can be found in the Supporting Information. This information is available free of charge via the internet at http://pubs.acs.org/.

References

1. Tian, N.; Zhou, Z.-Y.; Sun, S.-G.; Ding, Y.; Wang, Z. L., *Science* **2007,** *316,* 732.
2. Quan, Z.; Wang, Y.; Fang, J., *Acc. Chem. Res.* **2013,** *46,* 191.
3. Ford, L. P.; Nigg, H. L.; Blowers, P.; Masel, R. I., *J. Catal.* **1998,** *179,* 163.
4. Liu, Z. P.; Hu, P., *J. Am. Chem. Soc.* **2003,** *125,* 1958.
5. Baker, T. A.; Xu, B.; Jensen, S. C.; Friend, C. M.; Kaxiras, E., *Catal. Sci. Technol.* **2011,** *1,* 1166.
6. Yin, L.; Liebscher, J., *Chem. Rev.* **2007,** *107,* 133.
7. Antolini, E., *Energy Environ. Sci.* **2009,** *2,* 915.
8. Torborg, C.; Beller, M., *Adv. Synth. Catal.* **2009,** *351,* 3027.
9. Collins, G.; O'Dwyer, C.; Morris, M.; Holmes, J. D., *Langmuir* **2013,** *29,* 11950.
10. Zhang, Q.; Russell, T. P.; Emrick, T., *Chem. Mater.* **2007,** *19,* 3712.
11. Xu, S.-Y.; Ruan, Y.-B.; Luo, X.-X.; Gao, Y.-F.; Zhao, J.-S.; Shen, J.-S.; Jiang, Y.-B., *Chem. Commun.* **2010,** *46,* 5864.
12. Lamblin, M.; Nassar-Hardy, L.; Hierso, J.-C.; Fouquet, E.; Felpin, F.-X., *Adv. Synth. Catal.* **2010,** *352,* 33.
13. Choudary, B. M.; Madhi, S.; Chowdari, N. S.; Kantam, M. L.; Sreedhar, B., *J. Am. Chem. Soc.* **2002,** *124,* 14127.
14. Yuan, B.; Pan, Y.; Li, Y.; Yin, B.; Jiang, H., *Angew. Chem. Int. Ed.* **2010,** *49,* 4054.
15. LeBlond, C. R.; Andrews, A. T.; Sun, Y. K.; Sowa, J. R., *Org. Lett.* **2001,** *3,* 1555.
16. Han, W.; Liu, C.; Jin, Z., *Adv. Synth. Catal.* **2008,** *350,* 501.
17. Kim, S. W.; Kim, M.; Lee, W. Y.; Hyeon, T., *J. Am. Chem. Soc.* **2002,** *124,* 7642.
18. Lu, F.; Ruiz, J.; Astruc, D., *Tetrahedron Lett.* **2004,** *45,* 9443.

19. Collins, G.; Schmidt, M.; O'Dwyer, C.; Holmes, J. D.; McGlacken, G. P., *Angew. Chem. Int. Ed.* **2014,** *53,* 4142.
20. Crudden, C. M.; Sateesh, M.; Lewis, R., *J. Am. Chem. Soc.* **2005,** *127,* 10045.
21. Taladriz-Blanco, P.; Herves, P.; Perez-Juste, J., *Top. Catal.* **2013,** *56,* 1154.
22. Collins, G.; Blomker, M.; Osaik, M.; Holmes, J. D.; Bredol, M.; O'Dwyer, C., *Chem. Mater.* **2013,** *25,* 4312.
23. Hariprasad, E.; Radhakrishnan, T. P., *ACS Catalysis* **2012,** *2,* 1179.
24. Mohanty, A.; Garg, N.; Jin, R., *Angew. Chem. Int. Ed.* **2010,** *49,* 4962.
25. Wang, F.; Li, C.; Sun, L.-D.; Wu, H.; Ming, T.; Wang, J.; Yu, J. C.; Yan, C.-H., *J. Am. Chem. Soc.* **2011,** *133,* 1106.
26. Jin, M.; Zhang, H.; Xie, Z.; Xia, Y., *Angew. Chem. Int. Ed.*

2011, *50,* 7850.
27. Hong, J. W.; Kim, M.; Kim, Y.; Han, S. W., *Chem. Eur. J.* **2012,** *18,* 16626.
28. Chen, Y.-H.; Hung, H.-H.; Huang, M. H., *J. Am. Chem. Soc.* **2009,** *131,* 9114.
29. Yu, Y.; Zhang, Q.; Liu, B.; Lee, J. Y., *J. Am. Chem. Soc.* **2010,** *132,* 18258.
30. Tian, N.; Zhou, Z.-Y.; Sun, S.-G., *Chem. Comm.* **2009,** 1502.
31. Chen, Y.-X.; Lavacchi, A.; Chen, S.-P.; di Benedetto, F.; Bevilacqua, M.; Bianchini, C.; Fornasiero, P.; Innocenti, M.; Marelli, M.; Oberhauser, W.; Sun, S.-G.; Vizza, F., *Angew. Chem.-Int. Edit.* **2012,** *51,* 8500.
32. Tian, N.; Zhou, Z.-Y.; Yu, N.-F.; Wang, L.-Y.; Sun, S.-G., *J. Am. Chem. Soc.* **2010,** *132,* 7580.
33. Diaz Valenzuela, C.; Carriedo, G. A.; Valenzuela, M. L.; Zuniga, L.; O'Dwyer, C., *Sci. Rep.* **2013,** *3,* 2642.
34. Le Bars, J.; Specht, U.; Bradley, J. S.; Blackmond, D. G., *Langmuir* **1999,** *15,* 7621.
35. Li, Y.; Hong, X. M.; Collard, D. M.; El-Sayed, M. A., *Org. Lett.* **2000,** *2,* 2385.
36. Davis, J. J.; Bagshaw, C. B.; Busuttil, K. L.; Hanyu, Y.; Coleman, K. S., *J. Am. Chem. Soc.* **2006,** *128,* 14135.
37. Davis, J. J.; Coleman, K. S.; Busuttil, K. L.; Bagshaw, C. B., *J. Am. Chem. Soc.* **2005,** *127,* 13082.
38. Ellis, P. J.; Fairlamb, I. J. S.; Hackett, S. F. J.; Wilson, K.; Lee, A. F., *Angew. Chem. Int. Ed.* **2010,** *49,* 1820.
39. Pachon, L. D.; Rothenberg, G., *Appl. Organometal. Chem.* **2008,** *22,* 288.
40. Niu, Z.; Peng, Q.; Zhuang, Z.; He, W.; Li, Y., *Chem. Eur. J.* **2012,** *18,* 9813.
41. Gaikwad, A. V.; Holuigue, A.; Thathagar, M. B.; ten Elshof, J. E.; Rothenberg, G., *Chem. Eur. J.* **2007,** *13,* 6908.
42. Fang, P.-P.; Jutand, A.; Tian, Z.-Q.; Amatore, C., *Angew. Chem. Int. Ed.* **2011,** *50,* 12184.
43. Diallo, A. K.; Ornelas, C.; Salmon, L.; Aranzaes, J. R.; Astruc, D., *Angew. Chem. Int. Ed.* **2007,** *46,* 8644.
44. Adrio, L. A.; Nguyen, B. N.; Guilera, G.; Livingston, A. G.; Hii, K. K., *Catal. Sci. Technol.* **2012,** *2,* 316.
45. Thathagar, M. B.; ten Elshof, J. E.; Rothenberg, G., *Angew. Chem. Int. Ed.* **2006,** *45,* 2886.
46. de Vries, A. H. M.; Mulders, J.; Mommers, J. H. M.; Henderickx, H. J. W.; de Vries, J. G., *Org. Lett.* **2003,** *5,* 3285.
47. Gaikwad, A. V.; Rothenberg, G., *Phys. Chem. Chem. Phys.* **2006,** *8,* 3669.
48. Narayanan, R.; El-Sayed, M. A., *J. Phys. Chem. B* **2005,** *109,* 4357.
49. Widegren, J. A.; Finke, R. G., *J. Mol. Catal. A* **2003,** *198,* 317.
50. Collins, G.; Schmidt, M.; McGlacken, G. P.; O'Dwyer, C.; Holmes, J. D., *J. Phys. Chem. C* **2014,** *118,* 6522.
51. Ramezani-Dakhel, H.; Mirau, P. A.; Naik, R. R.; Knecht, M. R.; Heinz, H., *Phys. Chem. Chem. Phys.* **2013,** *15,* 5488.
52. Xue, L.; Lin, Z., *Chem. Soc. Rev.* **2010,** *39,* 1692.
53. Braga, A. A. C.; Ujaque, G.; Maseras, F., *Organometallics* **2006,** *25,* 3647.

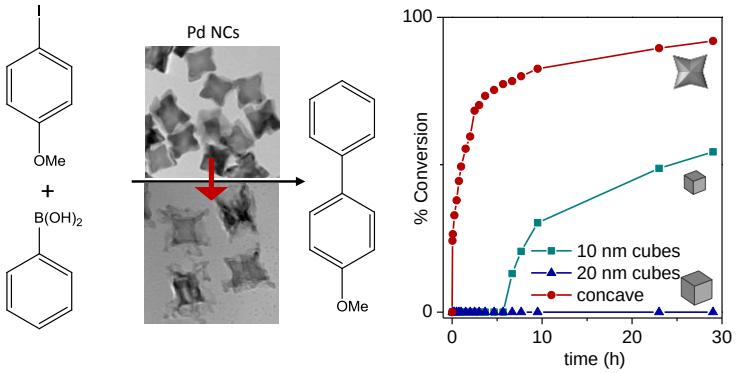
I
OMe
+
B(OH)2
Pd NCs
OMe
100
0
% Conversion
0
10
20
30
time (h)
10 nm cubes
20 nm cubes
concave